CO2 Separation from Flue Gas Using Polyvinyl-(Room Temperature Ionic Liquid)−Room Temperature Ionic Liquid Composite Membranes

ARTICLE *in* INDUSTRIAL & ENGINEERING CHEMISTRY RESEARCH · JULY 2011

Impact Factor: 2.59 · DOI: 10.1021/ie2005884

3 AUTHORS:

Pei Li
Beijing University of Chemical Technology
26 PUBLICATIONS **409** CITATIONS
SEE PROFILE

Pramoda Kumari
Agency for Science, Technology and Researc…
86 PUBLICATIONS **3,451** CITATIONS
SEE PROFILE

Tai-Shung Chung
National University of Singapore
726 PUBLICATIONS **19,531** CITATIONS
SEE PROFILE

I&EC research
Industrial & Engineering Chemistry Research

ARTICLE

pubs.acs.org/IECR

CO_2 Separation from Flue Gas Using Polyvinyl-(Room Temperature Ionic Liquid)−Room Temperature Ionic Liquid Composite Membranes

Pei Li,[†] K. P. Pramoda,[‡] and Tai-Shung Chung*[,†]

[†]Department of Chemical and Biomolecular Engineering, National University of Singapore, 10 Kent Ridge Crescent, Singapore 117602
[‡]Institute of Materials Research and Engineering, 3 Research Link, Singapore 117602

ABSTRACT: In this work, a vinyl-functionalized room temperature ionic liquid (RTIL), 1-vinyl-3-butylimidazolium bis(trifluoromethylsulfonyl)imide ([vbim][Tf_2N]), has been successfully synthesized. The RTIL was further polymerized and mixed with 1-butyl-3-methylimidazolium bis(trifluoromethylsulfonyl)imide ([bmim][Tf_2N]) to form the free-standing poly([vbim][Tf_2N])−[bmim][Tf_2N] composite films. The compositions of [bmim][Tf_2N] in the composite membranes were designed at 15, 30, 45, and 60 wt %. The pristine poly([vbim][Tf_2N]) and poly([vbim][Tf_2N])−[bmim][Tf_2N] composite membranes exhibit similar permeability selectivities as the standard [bmim][Tf_2N] but permeabilities are enhanced up to 5 times higher than the equivalent polystyrene-RTIL and polyacrylate-RTIL membranes. An increase in [bmim][Tf_2N] concentration of poly([vbim][Tf_2N])−[bmim][Tf_2N] composite membranes results in an increase in solubility, diffusivity, and permeability coefficients of CO_2 and N_2 but does not change the CO_2/N_2 selectivities of the solubility, diffusivity, and permeability. The CO_2 permeability of the 60 wt % composite at 35 °C, 10 atm is 559 barrers in pure gas tests which is closer to 60% of the [bmim][Tf_2N] permeability (i.e., 1344 barrers). In addition, the 60 wt % composite membrane exhibits a CO_2 permeability of 491.2 barrers and a CO_2/N_2 selectivity of 20 in mixed gas tests using CO_2/N_2 (50:50) as the feed.

1. INTRODUCTION

The increasing amount of CO_2 in the Earth's atmosphere, which is mainly due to the increase in the combustion of fossil fuels such as petroleum, natural gas, and coal,[1] is believed to be the key contributing factor to global warming. Therefore, there is an urgent requirement to sequester CO_2 from flue gas (gas generated from fossil combustion) before its release.[2] Current technologies to separate CO_2 include adsorption, absorption, membrane, and cryogenic separation.[2,3] Among these technologies, membrane separation exhibits inherent advantages including low energy consumption, small scale of equipment, environmentally benign, and ease to be incorporated with existing processes.[4] Thus, there is a great opportunity for the application of membrane technology in CO_2 separation.

RTIL has attracted much attention on applications for gas separation membranes, especially for CO_2 separation because RTIL can be designed to possess an extraordinary affinity to CO_2.[5−7] Supported ionic liquid membrane (SILM)[8−14] has been extensively studied because the characteristics of low volatility and high thermal stability of RTILs make themselves ideal liquid phases for supported liquid membrane applications. Some SILMs exhibited excellent separation performances for the CO_2/He gas pair with a selectivity of 3.1−8.7 and a CO_2 permeability of 744−1200 barrers.[9] In addition, the CO_2/N_2 selectivity of SILMs was in the range of 20−60.[13] However, the inherently weak mechanical stability of SILMs and relatively thick supported liquid membranes limit the operational transmembrane pressure and the membrane flux for useful industrial applications. An alternative attempt is to polymerize RTILs since poly(RTIL)s are in solid states which have better mechanical stabilities and thus can be fabricated into thin-layer membranes.

Reports on poly(RTIL) gas separation membranes started appearing 5 years ago. Some poly(RTIL)s exhibited higher CO_2 solubility and faster sorption/desorption rates compared to those of RTIL monomers.[15−17] These polymerizable RTILs were further copolymerized with ethylene glycol (EG) to improve the mechanical stability so that they could form free-standing poly(RTIL)-*co*-PEG copolymer films via the solution casting method.[18] These copolymers possessed good separation performances at 40 psi for the CO_2/N_2 gas pair that exceeded the 1991 "Robeson upper bound".[19] The good performance of poly(RTIL)-*co*-PEG copolymer is likely attributed to PEG since PEG itself has strong interactions with CO_2. In addition, the incorporation of PEG limited the RTIL concentration in the copolymer.

To study the gas separation properties of the "pure" poly(RTIL)s, Noble's group first coated styrene and acrylate functionalized RTILs on the surface of a porous polyethersulfone membrane (Super 200 PES membrane, Pall Corp., USA.) which provided the mechanical support to the RTILs then polymerized the RTILs using UV polymerization.[20,21] These membranes showed good performance at 2 atm for CO_2/N_2 which surpassed the 1991 "Robeson upper bound". Based on our best knowledge, the earlier reported CO_2 permeability of pure polystyrene-RTIL and polyacrylate-RTIL membranes were in the range of 5−30 barrers[20−24] and the CO_2 permeabilities of the SILMs were in the range of 200−1700 barrers.[25] The low permeability of these poly(RTIL)s was due to the large decrease in gas diffusivity after

Received: March 23, 2011
Accepted: June 23, 2011
Revised: May 28, 2011
Published: June 23, 2011

dx.doi.org/10.1021/ie2005884 | *Ind. Eng. Chem. Res.* 2011, 50, 9344–9353

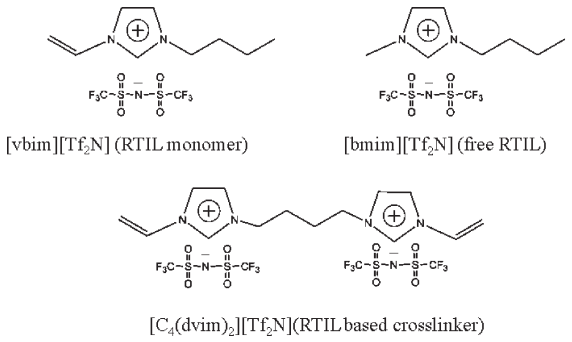

Figure 1. RTIL-based monomer, free RTIL, and cross-linker structures for synthesizing poly(RTIL)−RTIL composite films.

polymerization.[20] To overcome it, Bara et al. incorporated a "free" (i.e., unreactable) RTIL component into the poly(RTIL)s matrix to increase gas diffusivity. The CO_2 permeability in their polystyrene-based poly(RTIL) increased from 9.2 to 44 barrers while the CO_2/N_2 selectivity increased from 32 to 39 after the incorporation of 20 mol % [emim][Tf_2N].[26] These improvements inspired more studies on poly(RTIL)-RTIL composite films. The CO_2 permeability with 20 mol % free RTIL was increased to a range of 33−55 with CO_2/N_2 selectivity varying from 20 to 40.[22,27,28] However, gas separation results on poly(RTIL)−RTIL composite membranes were still limited.

For industrial gas separation, transport data at higher pressures for long-term performance are needed because certain applications such as CO_2 separation from natural gas usually require a higher operation pressure. In addition, the separation properties of the poly(RTIL)−RTIL composites with a higher RTIL composition have barely been reported. To the best of our knowledge, only one paper related to high concentration poly(RTIL)−RTIL−zeolite composites has been published.[29] In their work, a polyvinyl-RTIL, poly([vinylhexylimidazolium][Tf_2N]), was synthesized and exhibited a CO_2 permeability of 70 barrers; the poly(RTIL) containing 60 wt % free RTIL showed a CO_2 permeability of 286 barrers.[29]

Therefore, the objectives of this work are (i) to explore poly(RTIL)−RTIL composite membranes that possess a higher concentration of free RTIL; (ii) to molecularly design poly(RTIL)−RTIL composite membranes that exhibit a similar CO_2 permeability and CO_2/N_2 selectivity to those of SILM containing the same free RTIL; (iii) to fabricate composite membranes that are mechanically strong and suitable for tests under a transmembrane pressure of 10 atm; and (iv) to study the impact on physical properties including T_g, density, FFV, and transport properties of the poly(RTIL)−RTIL composite by incorporating free RTIL.

In this report, we have synthesized a series of new poly(RTIL)−RTIL composite films with a concentration of free RTIL ranging from 15 to 60 wt %. The structures of the vinyl-functionalized RTIL, divinyl-functionalized RTIL (cross-linker), and the free RTIL (composite) are shown in Figure 1. We chose 1-vinyl-3-butylimidazolium bis(trifluoromethylsulfonyl)amide ([vbim][Tf_2N]) as the pristine poly(RTIL) due to the higher flexibility of the polyethylene backbone compared to the polystyrene backbone. The reason behind synthesizing 1,4-di[3-vinylimidazolium]butane bis(trifluoromethylsulfonyl) imide ([C_4(dvim)$_2$][Tf_2N]) cross-linker was to improve the mechanical stability of the polyvinyl-RTIL while keeping the maximum concentration of [Tf_2N] anion in the polymer because of its high affinity to CO_2.[25] 1-Butyl-3-methylimidazolium bis(trifluoromethylsulfonyl) imide ([bmim][Tf_2N]) was chosen as the free RTIL owing to its high CO_2/N_2 separation performance and similar structure to the [vbim][Tf_2N]. As a result, it may form a miscible mixing with poly([vbim][Tf_2N]).

2. EXPERIMENTAL SECTION

2.1. Materials. Carbon dioxide, nitrogen, and helium were purchased from Soxal (Singapore) with purities higher than 99.99%. All the chemicals were purchased from Sigma-Aldrich (Milwaukee, WI) except for lithium bis(trifluoromethylsulfonyl)-imide ($LiTf_2N$) which was purchased from SynQuest Laboratories (Alachua, FL). All the chemicals were used as received without further purification.

2.2. Preparation of the Poly(RTIL)−RTIL Composite Films. *2.2.1. Monomer Preparation.* The RTILs used in this work including [bmim][Tf_2N], [vbim][Tf_2N], and [C_4(dvim)$_2$]-[Tf_2N] were synthesized using the quaternization reaction followed by an anion exchange reaction that was similar to the method reported in the literature.[30] A specific procedure is shown in Scheme 1. The structures of the RTILs were confirmed by ^{1}H NMR and ^{13}C NMR data.

1-Vinyl-3-butylimidazolium Bis(trifluoromethylsulfonyl)-amide ([vbim][Tf_2N]). Yield 79%; ^{1}H NMR (400 MHz, DMSO-d_6) δ 9.92 (s, 1H), 8.38 (s, 1H), 8.06 (s, 1H), 7.42 (dd, 1H), 6.10 (d, 1H), 5.43 (d, 1H), 4.29 (d, 2H), 1.85 (m, 2H), 1.28 (m, 2H), 0.88 (m 3H); ^{13}C NMR (100 MHz, DMSO-d_6) δ 14.09, 19.62, 31.96, 49.81, 109.65, 120.21, 121.45, 124.12, 129.62, 136.08.

1,4-Di[3-vinylimidazolium]butane Bis[(trifluoromethyl)-sulfonyl]imide ([C_4(dvim)$_2$][Tf_2N]). Yield 85%; ^{1}H NMR (400 MHz, DMSO-d_6) δ 9.21 (s, 2H), 7.90 (s, 2H), 7.72 (s, 2H), 7.26 (dd, 2H), 5.93 (d, 2H), 5.53 (d, 2H), 4.41(m, 4H), 2.12(m, 4H); ^{13}C NMR (100 MHz, DMSO-d6) δ 26.72, 49.79, 110.32, 120.36, 121.48, 123.49, 128.87, 135.03.

2.2.2. Poly(RTIL)−RTIL Composite Film Preparation. To synthesize the poly(RTIL)−RTIL composite film, 18 g of RTIL monomer ([vbim][Tf_2N]) was mixed with 2 g of the cross-linker ([C_4(dvim)$_2$][Tf_2N]). The mixture was divided into 5 parts. A different amount of RTIL ([bmim][Tf_2N]) was added to each part so that the concentration of [bmim][Tf_2N] varied from 0, 15, 30, 45, and 60 wt %. After that, 0.5 wt % of the photo initiator, 1-hydroxycyclohexylphenyl ketone, was added to each RTIL mixture with 10 mL of acetone to facilitate mixing. Acetone was removed by vacuum distillation before UV polymerization. To form a free-standing film, the RTIL mixture was carefully placed on the top of a silicon wafer and covered by a transparent glass. The thickness of the RTIL mixture was controlled by an aluminum spacer in between the silicon wafer and the glass. The wafer−RTIL−glass sandwich was exposed to 254 nm UV light from a UV cross-linker (BLX-E254) purchased from Vilber Lourmat Corp. (Marne-la-vallée Cedex1, France) with an intensity of 2 mW/cm^2 for 60 min. After the polymerization, the glass was gently separated from the silicon wafer and the free-standing poly(RTIL)−RTIL film was removed from the glass using a razor blade. The film was placed in a vacuum oven and heated at 50 °C overnight to remove the residual solvent. This procedure is a modification to the method reported by Bara et al.[22]

Scheme 1. Synthesis Procedure of the Vinyl-Functionalized RTIL with Tf_2N Anion

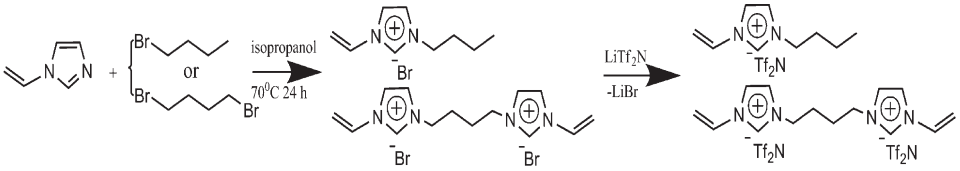

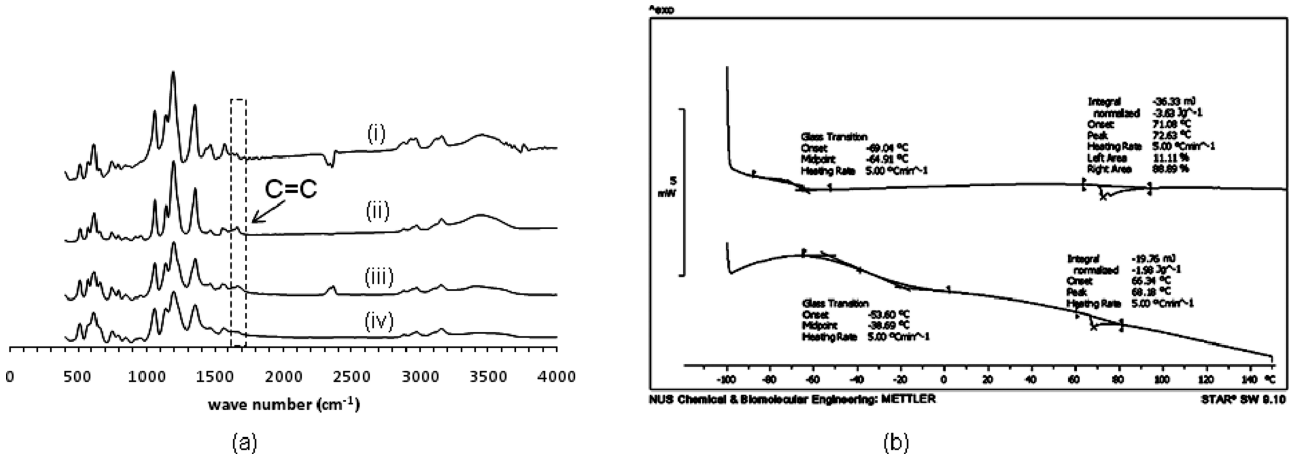

Figure 2. (a) FTIR spectra of (i) [bmim][Tf_2N], (ii) [vbim][Tf_2N], (iii) poly([vbim][Tf_2N]) synthesized using a soda-lime glass, and (iv) poly([vbim][Tf_2N]) synthesized using a quartz glass. (b) DSC spectra of poly([vbim][Tf_2N]) synthesized using a soda-lime glass (upper curve) and poly([vbim] [Tf_2N]) synthesized using a quartz glass (lower curve).

Scheme 2. Synthesis Procedure of Poly(RTIL)−RTIL Composite Films and Photos of the Pristine Poly([vbim]-[Tf_2N]), 15, 30, 45, and 60 wt % Poly([vbim][Tf_2N])−[bmim][Tf_2N] Composite Freestanding Films (from Left to Right)

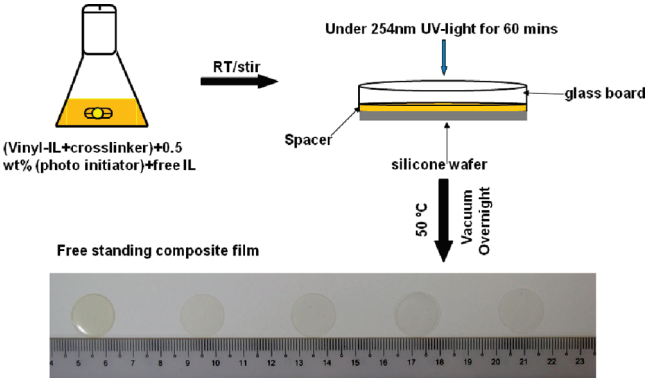

The type of glass covering the silicone wafer played a crucial role in UV polymerization. Initially, a soda-lime glass was used which caused a low conversion of the vinyl groups because a large part of the UV light was absorbed by the glass. Then, the soda-lime glass was replaced by a 5 cm × 5 cm × 2 mm quartz glass purchased from Shanghai Shengyuan Optical Glass Corp. (Shanghai, China) which allows 98% UV light to pass. A higher conversion was confirmed according to the FTIR spectroscopy given in Figure 2a. Both the [vbim][Tf_2N] monomer and the poly([vbim][Tf_2N]) synthesized using a soda-lime glass had a peak around 1650 cm^{-1} that represented the C═C stretching vibration. The peak showed a significant decrease for the poly([vbim][Tf_2N]) synthesized using a quartz glass. Based on the FTIR spectra, the conversion rates of the vinyl groups of the poly([vbim][Tf_2N]) synthesized using soda-lime and quartz glasses were 60% and 92%, respectively. Furthermore, according to the curves of differential scanning calorimetry (DSC) shown in Figure 2b, the poly([vbim][Tf_2N]) synthesized using a soda-lime glass exhibited a lower T_g than that of the polymer synthesized using a quartz glass. This arises from the fact that a lower conversion of the poly([vbim][Tf_2N]) would cause the poly([vbim][Tf_2N]) containing a large amount of free [vbim]-[Tf_2N] that enhances chain flexibility of the polymer and lowers its T_g.

Both the FTIR and the DSC results confirmed that UV polymerization via quartz glass is able to ensure a higher conversion of the vinyl groups. Freestanding films with a thickness ranging from 100 to 150 μm (as shown in Scheme 2) and a concentration of [bmim][Tf_2N] up to 60 wt % were therefore synthesized for further tests.

2.2.3. Characterization. The thicknesses from of the films were measured using a Digimatic indicator (IDC-112B-5) which was purchased from Mitutoyo Asia Pacific Pte. Ltd. (Japan) with an accuracy of 0.001 mm (1 μm). For every measurement, at least 5 points from different positions of each film were measured and the average value was referred to as the thickness.

The IR spectra of all samples were measured using a FTIR-8400 which was purchased from Shimadzu Corp. (Japan). The scan range was from 400 to 4000 cm^{-1}. The sample spectra automatically deducted the background spectra to get the IR

dx.doi.org/10.1021/ie2005884 |*Ind. Eng. Chem. Res.* 2011, 50, 9344–9353

Table 1. van der Waals Volume of Groups Used in This Study

group	V_w (cm^3/mol)
−H	3.44[a]
−CH−	6.79[a]
$-CH_2-$	10.23[a]
imidazole	54.2[b]
$[Tf_2N^-]$	90.8[c]

[a] Reference 32. [b] Reference 33. [c] Reference 34.

spectra. Since there was no nitrogen purge for this system, some CO_2 peaks would show up around 2400 cm^{-1}. The absorption peaks of the materials in the study do not appear at this position, and thus there is no effect on the analysis of the IR spectra.

The glass transition temperature (T_g) and melting point (T_m) of all samples were measured using a Mettler Toledo DSC 822e purchased from Mettler Toledo Inc. (Columbus, OH). The sample was first heated from room temperature to 150 °C at a rate of 5 °C/min and held at 150 °C for 2 min. After that, the sample was cooled down to −100 °C at a rate of 30 °C/min and then held for 2 min and heated to 150 °C at a rate of 5 °C/min. The T_g and T_m were acquired using the second heating curve. For each composition, three samples were tested and the variations of T_g and T_m were less than ±2 °C.

The densities of the films and [bmim][Tf_2N] were measured using a multipycnometer purchased from the Quantachrome Instruments (Boynton Beach, FL). The equipment allowed a known amount of helium under a pressure to be purged into a reference volume and then flowed into a sample cell which contained the testing material. The occupied volume of the material would be acquired using the pressure difference before and after helium flow into the sample cell via eq 1. The volume of the sample cell was 10.66 cm^3, and the sample volume was kept greater than 0.5 cm^3 to ensure accuracy. The pressure of helium was set at 19 psig when it was purged into the reference cell. All the density measurements were carried out at 28 °C (room temperature), and each sample was automatically measured 15 times to get the average value.

$$V_p = V_c - V_r\left[\left(\frac{P_1}{P_2}\right) - 1\right] \quad (1)$$

where V_p, V_c, and V_r are the volumes of sample, sample cell, and reference cell (the precise volume of the sample cell and reference cell are known), respectively. P_1 and P_2 are the pressures of helium in the reference cell and in the reference cell plus the sample cell, respectively. Consistent data have been observed between density data obtained from this density meter and density data from the literature for Matrimid 5218.

The fractional free volumes (FFV) of the pristine poly([vbim]-[Tf_2N]), poly([vbim][Tf_2N])−[bmim][Tf_2N] composites, and [bmim][Tf_2N] were estimated using eq 2.[31−35] The van der Waals volumes of all samples were estimated using the group contribution method.[32] The van der Waals volumes of groups used in this work are listed in Table 1.

$$FFV = \frac{V - V_0}{V} \quad (2)$$

where V is the specific volume (the molecular weight of the repeat unit of the polymer/density) of the polymer; V_0 is the volume occupied by the polymer molecules and V_0 equals 1.3 times of the polymer's van der Waals volume (V_w).

The CO_2 and N_2 sorption isotherms at 35 °C with pressure up to 10 atm were measured using a gravimetric technique via a Cahn D200 microbalance sorption apparatus.[36−38] The microbalance was first calibrated with individual gases including N_2 and CO_2 as a function of pressure. To perform a measurement, approximate 70 mg of a polymer film was placed into the sample pan. The system was evacuated overnight prior to test. N_2 or CO_2 was then purged into the system at different pressures up to 10 atm. At each pressure, the microbalance could measure the weight gain of the sample because of the gas sorption. Sorption is assumed to have reached equilibrium once there is no increase in the sample weight. From the weight gain, the amount of absorbed gas can be calculated by accounting the buoyancy correction.

The pure gas permeabilities of CO_2 and N_2 at 10 atm and 35 °C were measured by a constant-volume permeation cell using the standard method introduced in the literature.[38,39] The gas permeability was calculated using eq 3.[39]

$$P = \frac{273 \times 10^{10}}{760} \frac{VL}{AT \times \left(\frac{76}{14.7}\right) \times P_2}\left(\frac{dP_1}{dt}\right) \quad (3)$$

where P is the permeability coefficient of a film to a gas with an unit in barrer (1 barrer = 1×10^{-10} cm^3 (STP)-cm/cm^2 s cmHg), V is the volume of the downstream chamber (cm^3), L is the thickness of the membrane (cm), A refers to the effective area of the film (cm^2), T is the experimental temperature (K), P_2 is the upstream pressure (psia), P_1 is the downstream pressure (psia), and t is the time taken for the pressure (P_1) buildup.

The gas permeability of each sample was measured three times and the average value was presented with error bars. The diffusivities were calculated from the permeability and solubility data using eq 4.[31] The ideal selectivity was taken as the permeability ratio of the fast permeable gas to the slow permeable gas using eq 5.[31]

$$P = DS \quad (4)$$

where P, D, and S are the permeability, diffusivity, and solubility of the penetrant, respectively.

$$\alpha_{1,2} = \frac{P_1}{P_2} = \frac{S_1}{S_2}\frac{D_1}{D_2} = \alpha_S\alpha_D \quad (5)$$

where 1 refers to the fast permeable gas, 2 refers to the slow permeable gas, and $\alpha_{1,2}$, α_S, and α_D represent the ideal selectivities of permeability, solubility, and diffusivity, respectively.

The mixed gas permeability for CO_2/N_2 was measured for the 60 wt % composite film since it exhibited the best separation performance among all the composite films during pure gas tests. A binary gas mixture containing 50 mol % CO_2 and N_2 was used to measure the permeability at 10 and 20 atm at 35 °C. A gas chromatograph (Agilent 7890A) was used to analyze the molar composition of the permeate gas from the downstream of the permeation cell. The details of the equipment were introduced in a publication elsewhere.[36] The downstream pressure was kept lower than 10 Torr. When calculating gas permeability, the downstream pressure was assumed to be zero compared with the high pressure of the feed side. Therefore, the permeabilities of CO_2 and N_2 and the corresponding CO_2/N_2 selectivity of the mixed gas were

Table 2. T_g, T_m, Density,[a] FFV and [bmim][Tf_2N] Volume Percent of Poly(RTIL)−RTIL Films

	density (g/cm^3)	FFV	vol % of [bmim][Tf_2N]	T_g (°C)	T_m (°C)
poly(rtil)	1.5561 ± 0.0016	0.0848	0	−39 ± 1	68 ± 1
15 wt %	1.5335 ± 0.0022	0.0899	16.1	−48 ± 2	65 ± 2
30 wt %	1.5149 ± 0.0009	0.0947	32.0	−62 ± 2	62 ± 2
45 wt %	1.4970 ± 0.0018	0.0988	47.1	−73 ± 2	65 ± 2
60 wt %	1.4742 ± 0.0013	0.1041	62.2	−82 ± 1	49 ± 1
[bmim][Tf_2N]	1.4303 ± 0.0017	0.1145	100	−86[b]	−2[b]

[a] Density data were taken at 28 °C. [b] Data referred to ref 40.

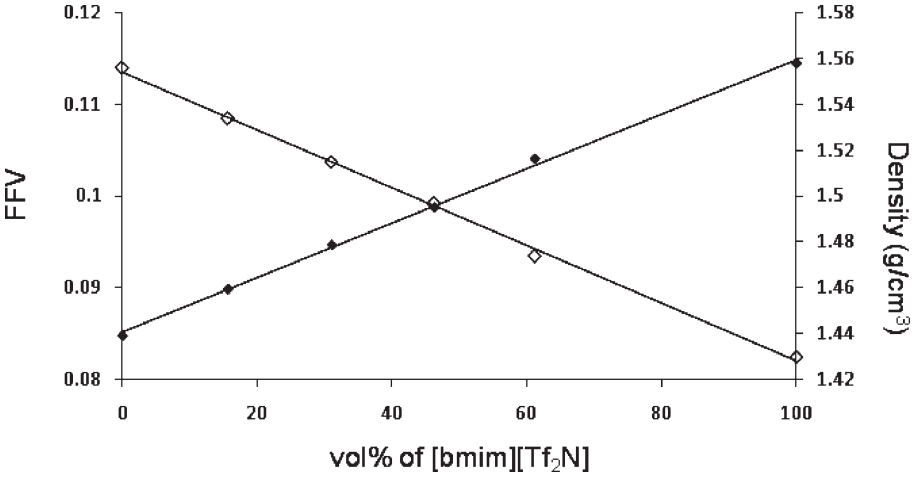

Figure 3. Density(◇) and FFV(◆) vs vol % of [bmim][Tf_2N] of the poly([vbim][Tf_2N])−[bmim][Tf_2N] composites.

calculated using eqs 6, 7, and 8.[36]

$$P_{CO_2} = P\frac{y_{CO_2}}{x_{CO_2}} \quad (6)$$

$$P_{N_2} = P\frac{y_{N_2}}{x_{N_2}} \quad (7)$$

$$\alpha_{CO_2/N_2} = \frac{y_{CO_2}/y_{N_2}}{x_{CO_2}/x_{N_2}} \quad (8)$$

where P is the permeability of the CO_2/N_2 mixed gas calculated using eq 3, P_{CO_2} and P_{N_2} are the permeabilities of CO_2 and N_2, respectively, y_{CO_2} and y_{N_2} are the molar fractions of CO_2 and N_2 of the permeate, respectively, x_{CO_2} and x_{N_2} are the molar fractions of CO_2 and N_2 of the feed, respectively, and α_{CO_2/N_2} is the CO_2/N_2 selectivity of the mixed gas.

3. RESULTS AND DISCUSSION

3.1. Physical Properties. FFV of a polymer is the fraction of volume not occupied by polymer chains.[32] FFV can be calculated by deducting the van der Waals volume from the specific volume (1/density) of a polymer. According to Figure 1, [vbim][Tf_2N] and [bmim][Tf_2N] have similar molecular structures; therefore, the estimated van der Waals volumes of the pristine poly([vbim][Tf_2N]) and [bmim][Tf_2N] are close (i.e., 202.94 versus 199.59 cm^3/mol). Since liquid [bmim][Tf_2N] has a smaller density than the pristine poly([vbim][Tf_2N]), the corresponding specific volume and FFV of the former are larger than those of the latter. The higher FFV of [bmim][Tf_2N] matches the general concept that liquids have more free volumes than polymers.[41] Therefore, the incorporation of [bmim][Tf_2N] into poly([vbim][Tf_2N]) would cause an increment in FFV and a decrease in density of the poly([vbim][Tf_2N])−[bmim][Tf_2N] composite as listed in Table 2. Figure 3 illustrates the correlations of the linearly increased FFVs and linearly decreased densities of poly([vbim][Tf_2N])−[bmim][Tf_2N] composites versus vol% of [bmim][Tf_2N]. The linear relations indicate a miscible mixing of the poly([vbim][Tf_2N])−[bmim][Tf_2N] composite.

Since T_g reflects the chain mobility of a polymer, a polymer with a high T_g may possess a low chain flexibility.[42] In addition, T_g can also be used to identify the phase behavior of polymer blends.[43] All poly([vbim][Tf_2N])−[bmim][Tf_2N] composites in this study only exhibit a single T_g, and all composite films shown in Scheme 2 are optically transparent; thus, the poly([vbim][Tf_2N])−[bmim]-[Tf_2N] composites should be homogeneous. As the pure [bmim]-[Tf_2N] has a much lower T_g than the pristine poly([vbim][Tf_2N]), an increase in [bmim][Tf_2N] concentration in the poly([vbim]-[Tf_2N])−[bmim][Tf_2N] composite leads to a decrease in T_g. In other words, the incorporation of [bmim][Tf_2N] not only increases the chain mobility of the resultant composites but also enhances their gas diffusivity and permeability. The detailed discussion of gas transport properties will be introduced later.

A cross-linked polymer usually cannot form crystals and melt. The observation of a melting point of the pristine poly([vbim]-[Tf_2N]) should be due to the residual "free" [vbim][Tf_2N] (since conversion is 92%) which formed crystals during the DSC cooling process. In the first heating process of the DSC experiment, the sample was heated from room temperature to 150 °C at a rate of 5 °C/min and no melting peak appeared. It indicates

dx.doi.org/10.1021/ie2005884 |Ind. Eng. Chem. Res. 2011, 50, 9344–9353

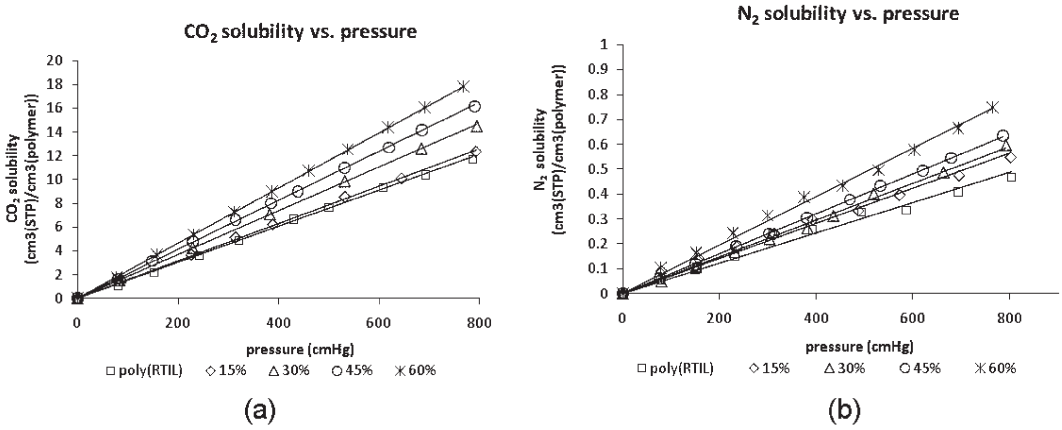

Figure 4. Sorption isotherms of CO_2 and N_2 of the poly([vbim][Tf_2N])−[bmim][Tf_2N] composites at 35 °C.

Table 3. Pure Gas *P*, *S*, and *D* Data of the CO_2/N_2 Gas Pair for the Plain Poly([vbim][Tf_2N]), Poly([vbim][Tf_2N])−[bmim]-[Tf_2N] Composites, and [bmim][Tf_2N]-Based SILM at 35 °C, 10 atm

	P^a			S^b			D^c		
	N_2	CO_2	CO_2/N_2	N_2	CO_2	CO_2/N_2	N_2	CO_2	CO_2/N_2
poly(RTIL)	4.55 ± 0.15	101.4 ± 0.5	22.3	0.61	15.1	24.7	0.75	0.67	0.91
15 wt %	6.20 ± 0.07	135.0 ± 0.8	21.8	0.70	15.6	22.3	0.89	0.88	0.98
30 wt %	11.8 ± 0.1	262.4 ± 0.5	22.2	0.76	18.3	24.0	1.56	1.44	0.93
45 wt %	15.0 ± 0.1	356.3 ± 1.3	23.3	0.81	20.1	24.6	1.86	1.78	0.95
60 wt %	21.6 ± 0.7	559.5 ± 1.8	25.9	0.95	23.3	24.4	2.27	2.40	1.06
[bmim][Tf_2N][d]	68.3	1344.3	19.7	1.2	26.8	23	5.89	5.02	0.85

[a] *P* in barrer (1 barrer = 10^{-10} (cm^3 STP) cm/cm^2 s $cmHg^{-1}$ [b] *S* in 10^3 cm^3(gas STP)/(cm^3(RTIL) cmHg). [c] *D* in 10^6 cm^2/s. [d] [bmim][Tf_2N] permeability data in the literature,[25] solubility data in the literature.[48]

that the sample does not containing any crystal initially. Crystals were formed when the sample was cooled down to −100 °C in the cooling process. Therefore, the impact of crystallinity on transport properties is negligible because the composite films did not contain any crystal during measurements of permeability and solubility.

3.2. Sorption Isotherms. Figure 4, a and b, illustrates the sorption isotherms of CO_2 and N_2 for the pristine poly([vbim]-[Tf_2N]) and poly([vbim][Tf_2N])−[bmim][Tf_2N] composites. The linear sorption curves indicate a typical Henry's type sorption and the values of slope can be referred to as the solubility coefficients, as summarized in Table 3. The CO_2 and N_2 solubilities in the pristine poly([vbim][Tf_2N]) are lower than those in pure [bmim][Tf_2N]. This phenomenon was also found by Lin et al.[41] who reported that poly(ethylene oxide) exhibited a lower CO_2 solubility than ethylene oxide due to a less free volume of poly(ethylene oxide) compared to the liquidlike ethylene oxide. Figure 5 depicts the linear relation between the CO_2 solubility coefficients and the FFVs of poly([vbim]-[Tf_2N])−[bmim][Tf_2N] composites. This result is consistent with Lin et al.'s observation.[41] The CO_2/N_2 solubility selectivities for all composites, pristine polymer, and pure [bmim]-[Tf_2N] are almost identical. Note that gas solubility in a polymer is affected by gas condensability, polymer free volume and polymer−gas interactions.[42] The unchanged CO_2/N_2 selectivity may imply similar gas−polymer/RTIL interactions between [bmim][Tf_2N] and poly([vbim][Tf_2N]).

3.3. Pure Gas Permeabilities and Diffusivities of CO_2 and N_2 in Poly([vbim][Tf_2N])−[bmim][Tf_2N] Composites. The gas transport properties in dense polymeric films can be interpreted using the solution-diffusion model. The gas permeability is governed by the combination of gas solubility and diffusivity. Diffusivity is affected by the size and shape of the penetrant, polymer chain flexibility, and polymer free volume.[42] Since the poly([vbim][Tf_2N])−[bmim][Tf_2N] composites are homogeneous, the permeability of the composites can be predicted using eq 9.[43−45]

$$\ln P_b = \Phi_1 \ln P_1 + \Phi_1 \ln P_2 \quad (9)$$

where P_b, P_1, and P_2 are the permeability coefficients of the blend and the pure components 1 and 2, respectively; Φ_1, and Φ_2 are the respective volume fractions of components 1 and 2, respectively.

Table 3 lists the *P*, *S*, and *D* along with the ideal selectivity of CO_2/N_2 gas pair. The CO_2 permeability at different volume percent of [bmim][Tf_2N] are compared with the estimated curve shown in Figure 6. The CO_2 permeabilities of all the composites lie on the estimated curve. It again proves that the composites are homogeneous polymer blends.

According to Table 3, both the solubilities and diffusivities of CO_2 and N_2 increase with an increase in [bmim][Tf_2N] concentration. However, the extent of increase in diffusivities is much greater than that in solubilities. This is due to the fact that the addition of [bmim][Tf_2N] greatly decreases T_g and significantly enhances chain mobility and diffusivity. As a result, the resultant poly([vbim][Tf_2N])−[bmim][Tf_2N] composites

dx.doi.org/10.1021/ie2005884 |*Ind. Eng. Chem. Res.* 2011, 50, 9344–9353

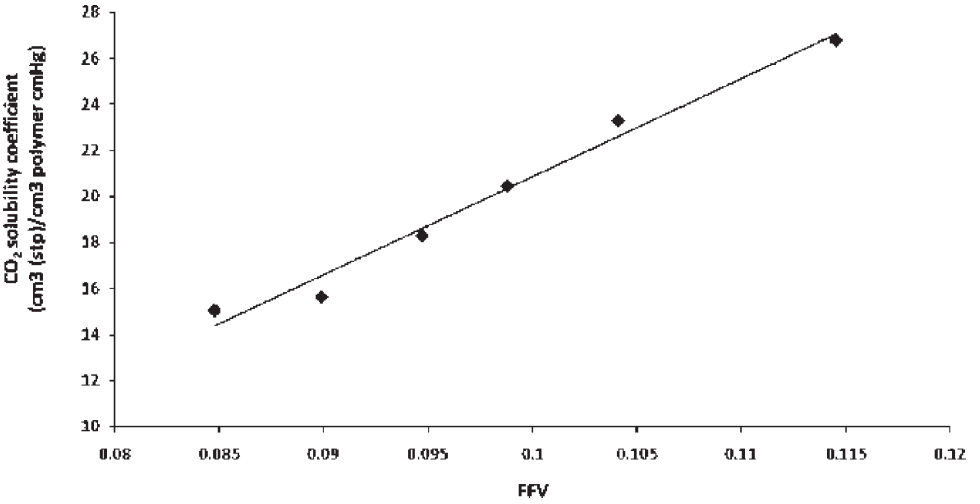

Figure 5. Solubility coefficient of CO_2 vs FFV of the poly([vbim][Tf_2N])−[bmim][Tf_2N] composites at 35 °C. (◇) 15 wt %; (◆) 0, 30, 45, 60 wt %, and pure [bmim][Tf_2N].

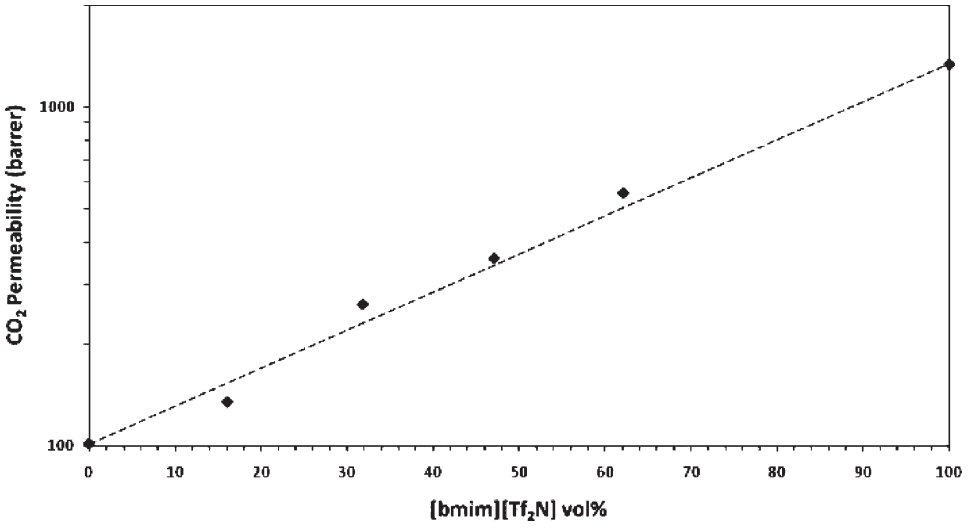

Figure 6. Comparison of the experimental values of CO_2 permeabilities (◆), with the estimated curve 1 using eq 8.

Table 4. Permeability and Selectivity of the 50/50 mol % CO_2/N_2 Mixed Gas of the 60 wt % Composite Film at 35 °C, 10 and 20 atm

	N_2	CO_2	CO_2/N_2
10 atm	24.4 ± 0.4	491.2 ± 5.5	20.0 ± 0.7
20 atm	38.9 ± 3.2	580.1 ± 3.3	14.9 ± 1.1

possess almost no size selectivity. The permeability selectivity is therefore controlled by solubility selectivity. Since the solubility selectivity of [bmim][Tf_2N] is similar to that of the pristine poly([vbim][Tf_2N]), the addition of [bmim][Tf_2N] increases the CO_2 permeability while maintaining the permeability selectivity.

3.4. Mixed Gas Permeability. The mixed gas permeability and selectivity data of the 60 wt % composite were tested using a mixed gas comprising 50/50 mol % CO_2/N_2 at 35 °C, 10 and 20 atm, and Table 4 summarizes the results. At 10 atm, the CO_2 permeability is lower than the ideal gas permeability, but the N_2 permeability is a little higher. It might be due to the effects of competitive sorption between the two gases and slightly CO_2-induced plasticization. Hert et al.[46] measured the solubility of a 50/50 mol % O_2/CO_2 mixed gas in 1-hexyl-3-methylimidazolium bis(trifluorosulfonyl)imide ([hmim][Tf_2N]). They found that the O_2 solubility in the mixed gas system at a total pressure of 10 bar was 4.9 times higher than the O_2 solubility in the pure gas system with the same O_2 fugacity at 25 °C. On the contrary, the CO_2 solubility in the mixed gas system (0.07 mol %) was less than the CO_2 solubility in the pure gas system (0.12 mol %). In addition, the sorption competition was enhanced by increasing the mixed gas pressure. Since [bmim][Tf_2N] has a similar structure to [hmim][Tf_2N] and N_2 typically possesses a little less but similar solubility to O_2, it is reasonable to assume that the sorption behavior of CO_2/N_2 mixed gas in poly([vbim]-[Tf_2N])−[bmim][Tf_2N] system is an analogue to that in the [hmim][Tf_2N] system. In other words, the CO_2 solubility would be less and the N_2 solubility would be greater in the CO_2/N_2

dx.doi.org/10.1021/ie2005884 |*Ind. Eng. Chem. Res.* 2011, 50, 9344–9353

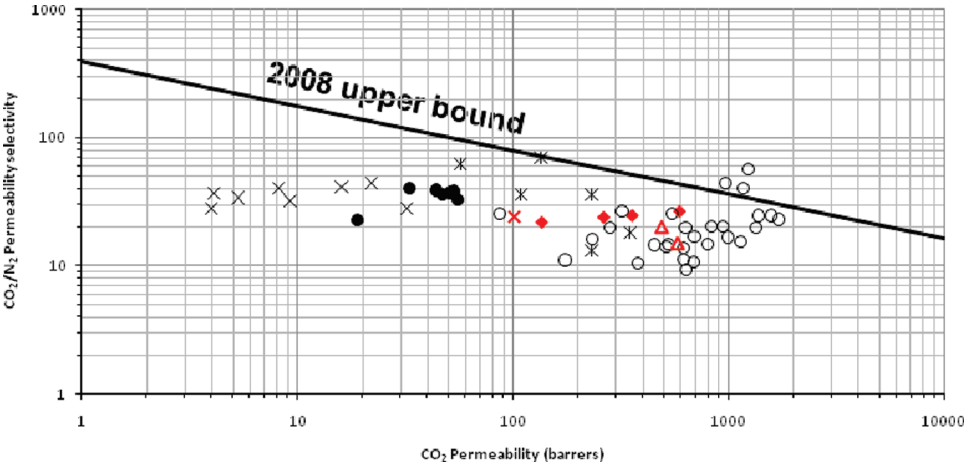

Figure 7. Separation performance of the CO_2/N_2 gas pair for different RTIL based membranes. Pure gas properties of (black ×) poly(RTIL);[21,26] (●) poly(RTIL)−RTIL composite with 20 mol % free RTIL;[22,26,27] (∗) poly(RTIL)−PEG copolymer;[18] (○) SILM;[25] (◆) poly([vbim][Tf_2N])−[bmim][Tf_2N] composite with [bmim][Tf_2N] concentration varied form 15, 30, 45, and 60 wt %; (red ×) pristine poly([vbim][Tf_2N]); and (△) the mixed gas properties (CO_2/N_2 50/50) of 60 wt % poly([vbim][Tf_2N])−[bmim][Tf_2N].

mixed gas system compared with those in the pure gas system at the same pressure and temperature. Furthermore, the sorption of CO_2 would plasticize the composite film and eventually increase the penetrate diffusivity. Therefore, CO_2 should exhibit a lower solubility and permeability, while N_2 a higher solubility and permeability at 10 atm due to the competitive sorption and plasticization. The CO_2-induced plasticization may become serious at 20 atm. As a result, the diffusivities and permeabilities of both CO_2 and N_2 increase, while both the solubility selectivity and permeability selectivity of the CO_2/N_2 gas pair decrease.

3.5. Comparison of Separation Performance. Figure 7 shows a comparison between the current works and key literature studies related to RTILs membranes using the "2008 Robeson Upper Bound" as a benchmark.[47] The poly([vbim][Tf_2N]) with polyethylene backbone exhibits a higher CO_2 permeability compared with the poly(RTIL)s with polystyrene or polyacrylate backbones. This might be due to the fact that the high chain flexibility of the polyethylene backbone leads to a higher diffusivity to CO_2. The poly([vbim][Tf_2N])−[bmim][Tf_2N] composite films exhibit a better separation performance than other poly(RTIL)−RTIL composites which have relatively low concentrations of free RTIL. The mixed gas performance is less impressive compared to the pure gas properties but is still promising with a CO_2 permeability of 491.2 barrers and a CO_2/N_2 selectivity of 20. In addition, the composite film is stable at a transmembrane pressure of 20 atm. The good mechanical stability may lead to a high-pressure application of poly(RTIL) membranes such as CO_2/CH_4 separation which is usually operated at a pressure above 30 atm. However, there is a challenge for poly(RTIL)−RTIL composites to go beyond the "upper bound of the CO_2/N_2 selectivity". This hurdle could be solved in the future by the incorporation of free RTILs which have higher CO_2/N_2 selectivities.

4. CONCLUSIONS

Poly([vbim][Tf_2N])−[bmim][Tf_2N] composites with [bmim][Tf_2N] concentration up to 60 wt % have been successfully synthesized and formed good free-standing films. All the films are mechanically stable at a transmembrane pressure of 10 atm. The poly(RTIL) and the free RTIL have formed miscible blends in a molecular level. Poly([vbim][Tf_2N]) with a polyethylene backbone exhibits a higher permeability to CO_2 (∼100 barrers) than poly(RTIL)s with the polystyrene or polyacrylate backbones. The incorporation of [bmim][Tf_2N] in the poly([vbim][Tf_2N]) results in a decrease in the T_g and an increase in the FFV, gas solubility, diffusivity, and permeability but maintains the CO_2/N_2 permeability selectivity compared with the pristine poly([vbim][Tf_2N]). It is found that the solubility selectivity plays the determining role in the CO_2/N_2 selectivity. The composite membrane containing 60 wt % [bmim][Tf_2N] exhibits the best separation performance of the CO_2/N_2 gas pair. The mixed gas properties of the 60 wt % composite indicates a competitive sorption between CO_2 and N_2 which causes decreases in the CO_2 permeability and CO_2/N_2 selectivity at 10 atm and a decrease in the CO_2/N_2 selectivity at 20 atm with an increase in the CO_2 permeability. The CO_2-induced plasticization may become serious at high pressures. Not only may it enhance CO_2 and N_2 diffusivities and permeabilities but also reduce their solubility selectivity and permeability selectivity.

AUTHOR INFORMATION

Corresponding Author

*E-mail: chencts@nus.edu.sg. Fax: (65)-67791936.

ACKNOWLEDGMENT

The authors thank the A*Star support for the project "Polymeric Membrane Development for CO_2 Capture from Flue Gas" (Grant No. R-398-000-058-305). Special thanks are dedicated to the colleagues in our group including Mr. Hangzhen Chen, Mr. Fuyun Li, Ms. Meiling Chua, and Ms. Huan Wang for the help in the sorption and permeation measurements and to Mr. Jincai Su and Mr. Cher Hon Lau for the help in the density measurement. P. Li also thanks Prof. Maria R. Coleman (University of Toledo, OH) and Prof. Jared L. Anderson (University of Toledo, OH) for leading me to the research fields of room temperature ionic liquids and membrane. Last but not the least, P. Li thanks Mr. Hamidreza (Nima) Hakimelahi (University of Toledo, OH) for the valuable suggestions to this work.

REFERENCES

(1) Standing, T. H. Climate Change Projections Hinge on Global CO(2), Temperature Data. *Oil Gas J.* **2001**, *99* (46), 20.

(2) Yang, H.; Xu, Z.; Fan, M.; Gupta, R.; Slimane, R. B.; Bland, A. E.; Wright, I. Progress in Carbon Dioxide Separation and Capture: a Review. *J. Environ. Sci.* **2008**, *20*, 14.

(3) Plasynski, S. I.; Chen, Z. Review of CO_2 Capture Technologies and Some Improvement Opportunities. *ACS Div. Fuel Chem. Prepr.* **2000**, *45* (4), 644.

(4) Stern, S. A. Polymers for Gas Separations: the Next Decade. *J. Membr. Sci.* **1994**, *94*, 1.

(5) Baltus, R. E.; Counce, R. M.; Culbertson, B. H.; Luo, H.; Depaoli, D. W.; Dai, S.; Duckworth, D. C. Examination of the Potential of Ionic Liquids for Gas Separations. *Sep. Sci. Technol.* **2005**, *40*, 525.

(6) Condermarin, R.; Scovazzo, P. Gas Permeabilities, Solubilities, Diffusivities, and Diffusivity Correlations for Ammonium-based Room Temperature Ionic Liquids with Comparison to Imidazolium and Phosphonium RTIL Data. *Chem. Eng. J.* **2009**, *147*, 51.

(7) Han, X.; Armstrong, D. W. Ionic Liquids in Separations. *Acc. Chem. Res.* **2007**, *40*, 1079.

(8) Fortunato, R.; Afonso, C. A. M.; Reis, M. A. M.; Crespo, J. G. Supported Liquid Membranes using Ionic Liquid: Study of Stability and Transport Mechanisms. *J. Membr. Sci.* **2004**, *242*, 197.

(9) Ilconich, J.; Myers, C.; Pennline, H.; Luebke, D. Experimental Investigation of the Permeability and Selectivity of Supported Ionic Liquid Membranes for CO_2/He Separation at Temperatures up to 125 °C. *J. Membr. Sci.* **2007**, *298*, 41.

(10) Ferguson, L.; Scovazzo, P. Solubility, Diffusivity, and Permeability of Gases in Phosphonium-based Room Temperature Ionic Liquids: Data and Correlations. *Ind. Eng. Chem. Res.* **2007**, *46*, 1369.

(11) Yokozeki, A.; Shiflett, M. B. Hydrogen Purification using Room-Temperature Ionic Liquids. *Appl. Energy* **2007**, *84*, 351.

(12) Scovazzo, P.; Kieft, J.; Finan, D. A.; Koval, C.; DuBois, D.; Noble, R. D. Gas Separation using Non-Hexafluorophosphate [PF6] Anion Supported Ionic Liquid Membranes. *J. Membr. Sci.* **2004**, *238*, 57.

(13) Scovazzo, P.; Havard, D.; McShea, M.; Mixon, S.; Morgan, D. Long-Term, Continuous Mixed-gas Dry Fed CO_2/CH_4 and CO_2/N_2 Separation Performance and Selectivities for Room Temperature Ionic Liquid Membranes. *J. Membr. Sci.* **2009**, *327*, 41.

(14) Bara, J. E.; Gabrel, C. J.; Carlisle, T. K.; Camper, D. E.; Finotello, A.; Gin, D. L.; Noble, R. D. Gas Separation in Fluoroalkyl-Functionalized Room-Temperature Ionic Liquids Using Supported Liquid Membranes. *Chem. Eng. J.* **2009**, *47*, 43.

(15) Tang, J.; Tang, H.; Sun, W.; Plancher, H.; Radosz, M.; Shen, Y. Poly(Ionic Liquid)s: a New Material with Enhanced and Fast CO_2 Absorption. *Chem. Commun.* **2005**, 3325.

(16) Tang, J.; Tang, H.; Sun, W.; Radosz, M.; Shen, Y. Poly(Ionic Liquid)s as New Material for CO_2 Absorption. *J. Polym. Sci., Part A* **2005**, *43*, 5477.

(17) Tang, H.; Tang, J.; Ding, S.; Radosz, M.; Shen, Y. Atom Transfer Radical Polymerization of Styrenic Ionic Liquid Monomers and Carbon Dioxide Absorption of the Polymerized Ionic Liquids. *J. Polym. Sci., Part A* **2005**, *43*, 1432.

(18) Hu, X.; Tang, J.; Blasig, A.; Shen, Y.; Radosz, M. CO_2 Permeability, Diffusivity and Solubility in Polyethylene Glycol-Grafted Polyionic Membranes and their CO_2 Selectivity Relative to Methane and Nitrogen. *J. Membr. Sci.* **2006**, *281*, 130.

(19) Robeson, L. M. Correlation of Separation Factor versus Permeability for Polymeric Membranes. *J. Membr. Sci.* **1991**, *62*, 165.

(20) Bara, J. E.; Lessmann, S.; Gabriel, C. J.; Hatakeyama, E. S.; Noble, R. D.; Gin, D. L. Synthesis and Performance of Polymerizable Room-Temperature Ionic Liquids as Gas Separation Membranes. *Ind. Eng. Chem. Res.* **2007**, *46*, 5397.

(21) Bara, J. E.; Gabriel, C. J.; Hatakeyama, E. S.; Carlisle, T. K.; Lessmann, S.; Noble, R. D.; Gin, D. L. Improving CO_2 Selectivity in Polymerized Room-Temperature Ionic Liquid Gas Separation Membranes through Incorporation of Polar Substituents. *J. Membr. Sci.* **2008**, *321*, 3.

(22) Carlisle, T. K.; Bara, J. E.; Lafrate, A. L.; Gin, D. L.; Noble, R. D. Main-Chain Imidazolium Polymer Membranes for CO_2 Separations: An Initial Study of a New Ionic Liquid-Inspired Platform. *J. Membr. Sci.* **2010**, *359*, 37.

(23) Simons, K.; Nijmeijer, K; Bara, J. E.; Noble, R. D.; Wessling, M. How Do Polymerized Room-Temperature Ionic Liquid Membranes Plasticize during High Pressure CO_2 Permeation? *J. Membr. Sci.* **2010**, *360*, 202.

(24) Bara, J. E.; Hatakeyama, E. S.; Gabriel, C. J.; Zeng, X.; Lessmann, S.; Gin, D. L.; Noble, R. D. Synthesis and Light Gas Separations in Cross-Linked Gemini Room Temperature Ionic Liquid Polymer Membranes. *J. Membr. Sci.* **2008**, *316*, 186.

(25) Scovazzo, P. Determination of the Upper Limits, Benchmarks, and Critical Properties for Gas Separations using Stabilized Room Temperature Ionic Liquid Membranes (SILMs) for the Purpose of Guiding Future Research. *J. Membr. Sci.* **2009**, *343*, 199.

(26) Bara, J. E.; Hatakeyama, E. S.; Gin, D. L.; Noble, R. D. Improving CO_2 Permeability in Polymerized Room-Temperature Ionic Liquid Gas Separation Membranes through the Formation of a Solid Composite with a Room-Temperature Ionic Liquid. *Polym. Adv. Technol.* **2008**, *19*, 1415.

(27) Bara, J. E.; Noble, R. D.; Gin, D. L. Effect of "Free" Cation Substituent on Gas Separation Performance of Polymer-Room-Temperature Ionic Liquid Composite Membranes. *Ind. Eng. Chem. Res.* **2009**, *48*, 4607.

(28) Bara, J. E.; Camper, D. E.; Gin, D. L.; Noble, R. D. Room-Temperature Ionic Liquids and Composite Materials: Platform Technologies for CO_2 Capture. *Acc. Chem. Res.* **2010**, *43*, 152.

(29) Hudiono, Y. C.; Carlisle, T. K.; LaFrate, A. L.; Gin, D. L.; Noble, R. D. Novel Mixed Matrix Membranes based on Polymerizable Room-Temperature Ionic Liquids and SAPO-34 Particles to Improve CO_2 Separation. *J. Membr. Sci.* **2011**, *370*, 141.

(30) Wilkes, J. S.; Zaworotko, M. J. Air and Water Stable 1-Ethyl-3-Methylimidazolium based Ionic Liquids. *Chem. Commun.* **1992**, *13*, 965.

(31) Paul, D. R.; Yampol'skii, Y. P. *Polymeric Gas Separation Membranes*; CRC Press: Boca Raton, FL, 1994.

(32) Bondi, A. *Physical Properties of Molecular Crystals, Liquids, and Glasses*; John Wiley & Sons, Inc.: New York, 1968.

(33) Constantino, U.; Massucci, M. A.; Ginestra, A.; Tarola, A. M.; Zampa, L. Intercalation of Hyterocyclic Compounds in á-Zirconium Phosphate: Imidazole, Benzimidazole, Histamine and Histidine. *J. Inclusion Phenom.* **1986**, *4*, 147.

(34) Park, J. Y.; Paul, D. R. Correlations and Prediction of Gas Permeability in Glassy Polymer Membrane Materials via a Modified Free Volume based Group Contribution Method. *J. Membr. Sci.* **1997**, *125*, 23.

(35) Katsuta, S.; Imai, K.; Kudo, Y.; Takeda, Y.; Seki, H.; Nakadoshi, M. Ion Pair Formation of Alklimidazolium Ionic Liquids in Dichloromethane. *J. Chem. Eng. Data* **2008**, *53*, 1528.

(36) Chen, H. Z.; Xiao, Y. C.; Chung, T. S. Synthesis and Characterization of Poly(ethylene oxide) containing Copolyimides for Hydrogen Purification. *Polymer* **2010**, *51*, 4077.

(37) Chung, T. S.; Chan, S. S.; Wang, R.; Lu, Z.; He, C. Characterization of permeability and sorption inMatrimid/C60 mixed matrix membranes. *J. Membr. Sci.* **2003**, *211*, 91.

(38) Xiao, Y.; Shao, L.; Chung, T. S.; Schiraldi, D. A. Effects of Thermal Treatments and Dentrimers Chemical Structures on the Properties of Highly Surface Cross-Linked Polyimide Films. *Ind. Eng. Chem. Res.* **2005**, *44*, 3059.

(39) Li, P.; Zhao, Q.; Anderson, J. L.; Varanasi, S.; Coleman, M. R. Synthesis of Copolyimides based on Room Temperature Ionic Liquid Diamines. *J. Polym. Sci., Part A* **2010**, *48* (18), 4036.

(40) Fredlake, C. P.; Crosthwaite, J. M.; Hert, D. G.; Aki, S. N. V. K.; Brennecke, J. F. Thermophysical Properties of Imidazolium-based Ionic Liquids. *J. Chem. Eng. Data* **2004**, *49*, 954.

(41) Lin, H.; Freeman, B. D. Material Selection Guidelines for Membranes that Removal CO_2 from Gas Mixtures. *J. Mol. Struct.* **2005**, *739*, 57.

(42) Wijmans, J. G.; Baker, R. W. The Solution Diffusion Model: A Review. *J. Membr. Sci.* **1995**, *107*, 1.

(43) Hirayama, Y.; Yoshinaga, T.; Kusuki, Y.; Ninomiya, K.; Sakakibara, T.; Tamari, T. Relation of Gas Permeability with Structure of Aromatic Polyimides. I. *J. Membr. Sci.* **1996**, *111*, 169.

(44) Liu, S. L.; Wang, R.; Liu, Y.; Chng, M. L.; Chung, T. S. Gas Transport Properties of 6FDA-Durene/2,6-diaminotoluene Copolyimides. *Polymer* **2001**, *42*, 8847.

(45) Robeson, L. M. *Polymer Blends: A comprehensive review*; Hanser Garden Publications: Cincinnati, OH, 2007; pp 253−315, 338−359.

(46) Hert, D. G.; Anderson, J. L.; Aki, S. N. V. K.; Brennecke, J. F. Enhancement of Oxygen and Methane Solubility in 1-Hexyl-3-Methylimidazolium Bis(trifluorosulfonyl) imide Using Carbon Dioxide. *Chem. Commun.* **2005**, 2603.

(47) Robeson, L. M. The Upper Bound Revisited. *J. Membr. Sci.* **2008**, *320*, 390.

(48) Bara, J. E.; Gabriel, J. C.; Lessmann, S.; Carlisle, T. K.; Finotello, A.; Gin, D. L.; Noble, R. D. Enhanced CO_2 Separation Selectivity in Olio(ethylene glycol) Functionalized Room-Temperature Ionic Liquids. *Ind. Eng. Chem. Res.* **2007**, *46*, 5380.